International Journal of Hydrogen Energy 53 (2024) 490–502

Contents lists available at ScienceDirect

International Journal of Hydrogen Energy

journal homepage: www.elsevier.com/locate/he

Doped activated carbons obtained from nitrogen and sulfur-containing polymers as metal-free catalysts for application in nitroarenes hydrogenation

Juan-José Villora-Picó [a,b], Gema Gil-Muñoz [a,b], Antonio Sepúlveda-Escribano [a,b], M. Mercedes Pastor-Blas [a,b,*]

[a] Laboratorio de Materiales Avanzados, Departamento de Química Inorgánica – Instituto Universitario de Materiales de Alicante, Universidad de Alicante, Apartado 99, E-03080, Alicante, Spain
[b] Laboratory of Advanced Materials, Department of Inorganic Chemistry –University Institute of Materials of Alicante, University of Alicante, P.O. Box 99, E-03080, Alicante, Spain

ARTICLE INFO

Keywords:
S-doped activated carbon
N-doped activated carbon
S/N-Co-doped activated carbon
Polytiophene
Polypyrrole
Polyaniline
Hydrogenation of nitroarenes

ABSTRACT

Activated carbons doped with nitrogen and/or sulfur have been obtained by pyrolysis followed of steam activation of a sulfur containing polymer (polythiophene) and two nitrogen-containing polymers (polyaniline and polypyrrole). These polymers were synthesized by oxidative chemical polymerization in aqueous media of their corresponding monomers.

The influence of the steam activation on the textural properties and surface chemistry of the carbons has been evaluated and their catalytic activity has been determined in the hydrogenation reaction of 1-chloro-4-nitrobenzene. The degree of conversion in the reaction depends on the development of adequate porosity in the activated carbon (which is determined by the activation conditions) together with the presence of heteroatoms that act as active catalytic sites, with S showing considerably greater effectiveness than N. A compromise between an acceptable level of doping with sulfur and an adequate porosity is necessary, which has been achieved in a carbon obtained from polythiophene pyrolyzed at 900 °C and steam activated at 800 °C for 4 h, with a specific surface area of 742 m^2/g and S content of 1.71 at%.

1. Introduction

Nitroarenes are widely used as pesticides, herbicides and explosives. They are toxic and represent a risk to human health as they can seriously harm kidneys, liver and nerves. They are frequently found in industrial effluents. Thus, removal of toxic nitroarenes from wastewater is an important environmental issue [1]. The transformation of the toxic nitroarenes into value-added compounds, such as anilines, which in turn, are intermediates for dyes, polymers and pharmaceuticals production in the chemical industry [2], is highly interesting [3]. Anilines are typically prepared by the catalyzed reduction of nitroarenes.

Although some reductants are capable of generating hydrogen in situ, such as hydrazine hydrate, its high toxicity and cumbersome handling make its application on an industrial scale difficult [4]. Formic acid [5] and sodium borohydride [6], are interesting for their ease of use, however, some drawbacks associated to secure handling of formic acid as well as sodium borate generation as byproduct of sodium borohydride, makes necessary the search for alternative reducing agents. Thus, catalytic hydrogenation using molecular hydrogen is the most economical, environmentally benign, efficient, and straightforward approach for the reduction of nitroarenes [7,8].

The reduction of nitroarenes to produce anilines require the use of a catalyst. Highly efficient heterogeneous catalysts are preferred to homogeneous catalysts due to the ease separation and recyclability of the former [9]. However, several scientific challenges remain, such as achieving the selective hydrogenation of the nitro groups when other groups, which should be retained to preserve products with high synthetic value, are present [10].

The reaction mechanism and corresponding active sites for the adsorption of the nitro group, hydrogen dissociation and subsequent

* Corresponding author. Laboratorio de Materiales Avanzados, Departamento de Química Inorgánica – Instituto Universitario de Materiales de Alicante, Universidad de Alicante, Apartado 99, E-03080, Alicante, Spain
E-mail address: mercedes.pastor@ua.es (M.M. Pastor-Blas).

https://doi.org/10.1016/j.ijhydene.2023.12.005
Received 3 October 2023; Received in revised form 24 November 2023; Accepted 2 December 2023
Available online 9 December 2023

step-by-step hydrogenation are still under debate. H_2 activation is a critical step in the catalytic hydrogenation. This can be produced by homolytic or heterolytic dissociation [11]. The first involves the cleavage of the H–H bond and the formation of two hydrides. In this process, the metal catalyst accepts the σ electrons from H_2 and provides d-electrons to its antibonding σ* orbital. The other way to activate H_2 is through heterolytic dissociation, where H_2 is cleaved into $H^{\delta+}$ and $H^{\delta-}$ under the action of a nucleophile. Then, the hydrogenation of polar groups such as the nitro (-NO_2) group occurs.

In addition to H_2 dissociation, the adsorption and activation of the –NO_2 group are also critical to control the reaction selectivity. Selective hydrogenation of –NO_2 group in the presence of other reducible groups is a particular challenge, so the development of suitable catalysts is required. Many methods used to date, either cannot be considered as chemically sustainable or produce an improvement in selectivity at the expenses of activity. Thus, they are not satisfactory for practical applications [11]. It is therefore necessary to develop suitable catalysts, which are environmentally friendly, economically worthy, as well as highly selective to the hydrogenation of the nitro group of nitroarenes to give the corresponding aniline.

Catalysts based on precious, non-precious, mono- and bimetallic metals [12] have been extensively studied. Highly active metal catalysts for the hydrogenation reaction such as Pt [9,13–15], Pd [16–18], Rh [19], Ru [20] or Ni [11] generally have low selectivity towards the –NO_2 group in the presence of one or more additional reducible groups, especially the halogen group (F, Cl, Br and I) [21]. In the case of halonitroarenes, it is very common to obtain a mixture of haloanilines and dehalogenated products [9] at the experimental conditions required to obtain high conversion rates [8].

Although some satisfactory results have been obtained with non-noble metal catalysts such as Co [22] Ni [12] or Fe [23], they usually show low catalytic activity unless a promoter is added, and they suffer from irreversible deactivation due to the surface oxidation of metal particles. Besides, the problem of metal leaching into the solution makes necessary the search for metal-free alternatives.

The use of activated carbons not only as catalysts supports [24–26] but also as metal-free catalysts [27,28] has recently experienced an increasing interest. Non functionalized activated carbons are not suitable catalysts for the hydrogenation of nitroarenes because the interaction of the carbon surface with H_2 and the –NO_2 group is very weak due to the uniform charge distribution in the carbon material that abates the interaction between the reactants and the catalyst, and blocks the electron transfer [10,29]. Doping with heteroatoms [30] improves the properties of activated carbons resulting in enhanced thermal stability [31] and resistance against oxidation [32]. Doping also changes the electronic structure [33] of the carbon materials favoring their use as metal-free catalysts with adequate activities and selectivities [34]. The introduction of the heteroatom into the sp^2 structure of carbon modifies its electrical and chemical properties. Heteroatom binding to the carbon structure introduces new defects in nearby sites due to differences in bond length and atomic size between the dopant and the carbon atoms. This produces a local charge enrichment around the defect sites which favors H_2 dissociation.

Nitrogen doping has become popular in the recent decades [35,36]. N atom size (0.65 Å) is similar to that of C atom (0.70 Å), so it is easily inserted into the carbon lattice. Furthermore, the lone pair of electrons in the N atom can form π-conjugate bonds with π-bonds of the carbon lattice [29]. Because of the larger electronegativity of N atoms (3.04) with respect to that of C atoms (2.55), charge redistribution on the C atoms near the N dopant leads to an electron deficient area, which enhances hydrogen adsorption, and consequently increases the carbon catalytic performance [29,37–39].

Different N species are frequently observed in the nitrogen-doped carbon lattice: pyrrolic nitrogen, pyridinic nitrogen, graphitic nitrogen (also known as N-quaternary) and pyridine N-oxide (Scheme 1) [40]. Each of these species modifies the electronic and transport properties of carbon in a different way [41]. Pyridinic N is coordinated to two carbon atoms and contributes with one p electron to the π system, while pyrrolic N substitutes one carbon atom in a five-membered ring and contributes with two p electrons to the π system. Quaternary or graphitic nitrogen is found bonded to three carbon atoms in the hexagonal ring planes of carbon. Because it satisfies a lower number of coordination sites in this arrangement, it is expected to act as an electron donor. In addition to these nitrogen species, it is also possible to find oxidized nitrogen species (pyridine N-oxide). Different N species play a crucial role in different catalytic processes.

Although nitrogen has been extensively studied, there is a recent interest in sulfur doping of carbon [42,43], mainly for its application in electrochemical processes, due to the unique properties that sulfur provides to the carbon materials [44]. Sulfur [45] has an electronegativity (2.58) quite similar to carbon (2.55) but its size (1 Å) is considerable larger than that of carbon (0.70 Å) and nitrogen (0.65 Å). The introduction of sulfur atoms tends to induce structural defects in the carbon structures, which endows the carbon materials with unique electronic configurations, high specific surface areas and numerous active sites, which makes them very interesting in catalysis [46].

Among the different functionalities found in sulfur-doped carbons (Scheme 1) [40], some of them have a marked redox character, such as sulfone and sulfoxide groups, which are attributed to the improvement in the electrochemical properties of these carbons for their use in supercapacitors [40]. The most oxidized species (sulfoxide, sulfone or sulfonic acid) tend to be reduced to thioether or thiophene at high temperatures. In the thioether group, sulfur replaces one carbon atom within a six-atom ring and is bonded to two carbon atoms [47]. In the thiophene group, sulfur replaces one carbon atom in a five-atom cycle.

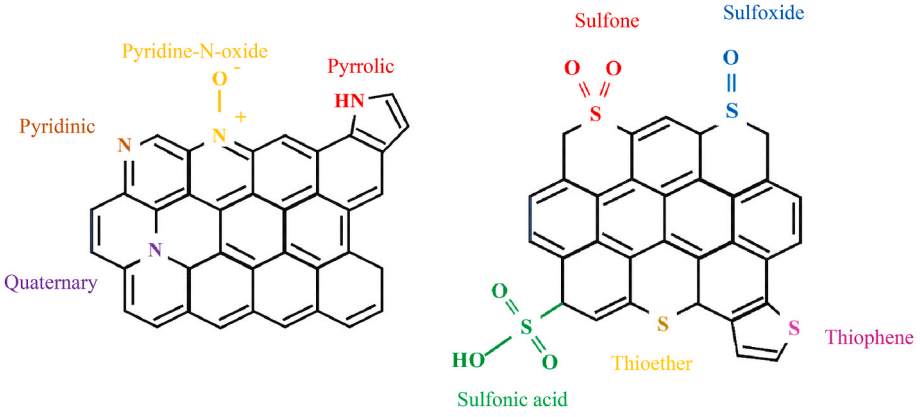

Scheme 1. N and S functionalities that can be detected in doped carbons.

There is much controversy about which nitrogen or sulfur species are active for the hydrogenation of nitroarenes. There are studies [48] that consider that oxidized nitrogen species and pyridinic nitrogen are not active for hydrogenation, and that the observed improvement in activity with increasing graphitic (quaternary) nitrogen content is indicative of the predominant role of this species in hydrogenation. This is explained by considering that the introduction of quaternary nitrogen into the carbon lattice provides carbon with a d-band electronic structure similar to that of metals, which makes the catalytic performance of carbon similar to metals [49]. However, Li et al. [29] attribute the selectivity of an N-doped carbon to the increasing in the pyrrolic nitrogen content to an adequate level, which generates a synergistic effect with graphitic nitrogen. Furthermore, they consider nonpolar hydrogen radicals to be the active species.

On the other hand, Xiong et al. [50] conclude that pyrrolic nitrogen is the most active species, which facilitates the heterolytic dissociation of hydrogen into $H^{\delta+}$ and $H^{\delta-}$. The reduction of nitrobenzene occurs by two pathways: the direct pathway with N-phenylhydroxylamine as the intermediate product, and the indirect pathway with azobenzene as the intermediate product [11]. In the mechanism they propose, $H^{\delta+}$ interacts with pyrrolic nitrogen and the neighboring carbons combine with $H^{\delta-}$. Next, nitrobenzene adsorbed on the carbon surface is reduced and hydrogenation occurs via the direct route.

Besides, Hu et al. [42] studied the catalytic reduction of nitrobenzene using hydrazine hydrate (N_2H_4) as hydrogen source and a N, S-co-doped catalyst prepared from a mixture of trithiocyanuric acid, glyoxal and melamine. They propose a mechanism in which N_2H_4 is adsorbed on the catalyst and further activated at the N- and S-containing active sites. Then the heterolytic cleavage of N_2H_4 is produced. The resulting hydrogen species bond with electronegative N and S (N–$H^{\delta+}$ and S–$H^{\delta+}$) and with electropositive C (C–$H^{\delta-}$). In addition, based on the above detailed analysis of N, S dopants and the formation of defects, the main active sites are located at defects. Then, nitrobenzene is reduced by the assistance of N–H $^{\delta+}$, S–H $^{\delta+}$, and C–H $^{\delta-}$ species at the defects, where the active sites are preferably located.

Sulfur-doped carbons can be prepared directly from different sulfur-containing precursors. Sulfur can be added in a post-treatment as well, by making the carbon react with a sulfur-rich compound in the form of either a gas [44], a liquid or a solid [51,52]. The former method produces carbons with a high doping level and a very good distribution of sulfur in the material [53], while the procedure based on mixing the carbon with a sulfur precursor may block part of the porosity, thus decreasing the carbon surface area. Besides, sulfur that is not incorporated into the carbon lattice can easily leach to the solution, which is a detrimental consequence [54,55].

Taking this into account, in this work, an alternative method for obtaining sulfur-doped carbons has been considered. It is based on the pyrolysis of a sulfur-containing polymer, polythiophene. Polythiophene is a conducting polymer, although its interest in this work is not related to its electrical properties but to the regular distribution of sulfur in its polymeric structure. It can be synthesized either electrochemically or chemically, although the later produces a higher yield. Chemical synthesis is based on the oxidative polymerization of thiophene monomer usually in organic solvents, due to the low solubility of thiophene in water [56,57]. In order to avoid the environmental concerns inherent to this synthesis, an alternative environmentally friendly route in aqueous medium has been used in this work, which is quite challenging due to the low solubility of thiophene in water [58].

Sulfur-doped carbons have been used as metal phase-free catalysts in both oxidation and reduction reactions. For example, Anfar et al. [59] prepared sulfur-doped carbons from almond shells and compared their catalytic activity in the oxidation with sodium persulfate of various organic pollutants found in wastewater such as Orange G, Bisphenol A and Diuron. They found that the S-doped porous carbons were less active than the N or the N,S-doped carbons and that high levels of S in the carbon network negatively influenced the persulfate activation. On the other hand, Wang et al. [60] prepared sulfur-doped graphene using elemental sulfur. They found that a S content of 3.4 at.%, provided a high catalytic performance in the reduction of 4-nitrophenol to 4-aminophenol using sodium borohydride as reductant.

The benefits of doped carbon materials depend not only on the presence of heteroatoms, but also on the ability of the reactants to access the catalytic sites, especially in reactions involving the use of large molecules. For this reason, it is necessary to develop an adequate porosity. Polythiophene synthesized for this study was submitted to a pyrolysis treatment which resulted in a sulfur-containing carbon with very low porosity. Therefore, a further activation treatment was necessary. Steam activation under different experimental conditions of a the polytiophene-derived carbon were studied, and its physical and chemical properties evaluated.

There are very few studies involving the use polymers as precursors of doped carbons for their application as metal-free catalysts for the hydrogenation reaction of nitroarenes. Having in mind the use of green and sustainable procedures, the catalytic performance of the polythiophene-derived S-doped carbon in the hydrogenation of 1-chloro-4-nitrobenzene using the benign molecular hydrogen have been compared to those of N-doped carbons obtained from polyaniline and polypyrrole and to that of a N–S doped carbon obtained from the pyrolysis of polypyrrole-*co*-polythiophene copolymer. In all cases the polymers were chemically synthesized in aqueous media under environmentally friendly reaction conditions.

2. Experimental

2.1. Synthesis of the carbon materials

Polythiophene (PT) was synthesized by the oxidative polymerization of thiophene monomer in aqueous medium. This synthesis requires a combination of anhydrous $FeCl_3$ as catalyst and H_2O_2 as oxidant to guarantee a high yield, thanks to the continuous regeneration of Fe^{3+} by oxidation of the Fe^{2+} formed by reaction with H_2O_2 [58]. The $FeCl_3/H_2O_2$ ratio was 0.00422. The experimental procedure was as follows: 5.7 mL of thiophene monomer (C_4H_4S, Sigma Aldrich, ACS reagent, ≥99 %) were dissolved in 180 mL of distilled water and added to a glass reactor fitted with a reflux condenser and a mechanical stirrer. Hydrogen peroxide (33.75 mL, 30 % w/w, Sigma Aldrich, ACS Reagent, >99 %) was added to the reactant mixture solution. 48.0 mg of anhydrous iron (III) chloride ($FeCl_3$, Sigma Aldrich, ≥99.99 %) were dissolved in 15 mL of deionized water and slowly added to the reactant mixture solution with a syringe during 60 min. This mixture was then stirred at 300 rpm for 12 h at 50 °C. The initial colorless solution turned to orange and finally brown, indicating the polymerization process. The dark brown PT precipitated was washed with distilled water, filtered, and dried at 50 °C for 24 h.

Polypyrrole (PPy) was prepared by the oxidative polymerization of pyrrole monomer (C_4H_5N, Sigma Aldrich, ACS reagent, ≥99.5 %) using iron (III) chloride hexahydrate ($FeCl_3 \cdot 6H_2O$, Sigma Aldrich, ACS reagent, ≥99.5 %) as oxidant, in a molar ratio (oxidant:monomer) of 2.33. The oxidant (9 g, i.e. 0.033 mol) was dissolved in distilled water (200 mL) and then 1 mL of pyrrole monomer (i.e. 0.0144 mol) was added dropwise under stirring for 6 h at room temperature. The solution turned dark, this indicating the progress of the polymerization reaction. The precipitated PPy polymer was then filtered from the solution and washed with distilled water until the washing water turned colorless. Finally, PPy was dried in an oven at 80 °C for 12 h [61].

Polyaniline (PANI) was synthesized via oxidative chemical polymerization of aniline ($C_6H_5NH_2$, Sigma Aldrich, ACS reagent, ≥99.5 %). For the synthesis of polyaniline, ammonium peroxodisulfate was used as oxidant, so 14.8 g of $(NH_4)_2S_2O_8$ (Sigma Aldrich, ACS reagent ≥98 %) were dissolved in 300 mL of a sulfuric acid solution 0.2 M (H_2SO_4, Sigma Aldrich, ACS reagent, 95.0–98.0 %). Then 4 mL of aniline were added dropwise and the solution was stirred for 20 h at room temperature.

After approximately 30 min, the solution acquired a dark green color that confirmed the formation of the emeraldine salt form of the polymer. The PANI product was then filtered, washed with distilled water until yellowish washing waters turned colorless and finally dried at 80 °C for 12 h [62].

The synthesis of the PPy-PT copolymer was carried out by dissolving 2.8 mL of pyrrole and 2.8 mL of thiophene in 180 mL of water. Then, 33.75 mL of 30 % H_2O_2 was added to the mixture. Subsequently, 48 mg of $FeCl_3$ were dissolved in 15 mL of deionized water and slowly added dropwise for more than 60 min to the reaction mixture solution using a syringe. This mixture was stirred at 300 rpm for 12 h at 50 °C.

The synthesized polymers were pyrolyzed in a tubular furnace at 900 °C for 4 h using a heating ramp of 5 °C/min under a nitrogen flow (100 mL/min). The resulting carbons exhibited low porosity and surface area, so an activation treatment with steam was carried out to improve their porous properties. Thus, the carbons were introduced into a tubular oven equipped with a peristaltic pump and a drop of water was added every 4 min. This steam activation treatment was carried out at 800 °C for 4 h in the case of the carbons obtained from PPy and PANI. The carbon prepared from PT was submitted to steam activation at several temperatures (700, 800 and 900 °C) and activation times (4 or 6 h).

The following nomenclature was used for the activated carbons prepared from the carbonized polymers. First, the polymer is named with its acronym, then P refers to pyrolysis, the number refers to the pyrolysis temperature in Celsius degrees divided by 100; S refers to Steam activation, followed by a number that corresponds to the activation temperature in Celsius degrees divided by 100. The last number indicates the activation time in hours. For instance, sample PT-P9-S8-4 is a carbon obtained from polythiophene (PT), Pyrolyzed at 900 °C (9) and activated with Steam (S) at 800 °C (8) for 4 h (4).

2.2. Catalytic tests

The catalytic behavior of the metal-free doped carbon materials prepared from the polymers was tested in the 1-chloro-4-nitrobenzene hydrogenation reaction. The reaction was performed in a high-pressure stainless-steel reactor (Biometa), equipped with a hydrogen inlet, a stirrer, a furnace, pressure and temperature controllers and a system for aliquots extraction. 500 mg of carbon were added to 100 mL of a solution (0.1 M) of 1-chloro-4-nitrobenzene ($ClC_6H_4NO_2$, Sigma Aldrich, 99 %) in ethanol. Octane (200 μL) ($CH_3(CH_2)_6CH_3$, Sigma Aldrich, ≥99 %) was added as internal standard. Experimental conditions were set using H_2 at 50 bar. The system was heated under slight stirring rate (10 rpm) until a temperature of 150 °C was reached. At that time, the stirring rate was increased to 300 rpm. Finally, aliquots of 2 mL were periodically extracted and analyzed in a gas chromatograph (QP-2010 GC-MS Shimadzu) coupled to a mass spectrometer and an HP-5 capillary column using helium as carrier gas.

Each doped carbon sample was tested five times in the hydrogenation reaction, and the average of the conversion data was calculated. The standard deviation was always less than 2 % (Table S1). The reusability of metal-free doped carbon materials was studied on the PT-P9-S8-4 carbon sample for 5 cycles. Thus, the metal-free catalyst was recovered by filtration after each reaction cycle, washed with ethanol and dried in an oven at 80 °C for 6 h, before being reused.

2.3. Characterization techniques

The as-synthesized polymers were analyzed by Fourier Transform Infrared Spectroscopy in the Attenuated Total Reflection mode, (ATR-FTIR). A JASCO FTIR 4700 spectrometer equipped with an ATR PRO ONE accessory was used. The analysis was performed using a scanning speed of 2 mm/s, an aperture of 7.1 mm and a resolution of 4 cm^{-1}.

TGA experiments were carried out in a TGA-DSC2 (Mettler Toledo) equipment. A heating rate of 10 °C/min and a nitrogen flow of 100 mL/min were set. A sample mass of 3–4 mg was introduced into a 70 μL alumina crucible, which was allowed to stabilize for 20 min at room temperature. A temperature scan between 25 and 900 °C was performed.

The textural properties of the carbons were determined by N_2 and CO_2 adsorption measurements at −196 °C and 0 °C, respectively, using an AUTOSORB-6 equipment (Quantachrome Instruments). The samples were previously outgassed at 250 °C for 4 h under vacuum in an AUTOSORB DEGASSER (Quantachrome Instruments).

SEM images were obtained with a Hitachi S3000 N scanning microscope. Previously to the measurement, the samples were dried in an Electron Microscopy Sciences model EMS 850 critical point drier.

X-ray photoelectron spectroscopy (XPS) was performed in a K-ALPHA spectrometer (Thermo Scientific). All spectra were collected using Mg-K_α radiation (1253.6 eV), monochromatized by a twin crystal monochromator, yielding a focused X-ray spot with a diameter of 400 nm, at 3 mA x 12 Kv.

Raman spectroscopy was carried out in a Raman Jasco NRS-5100 equipment using a 532 nm laser and 600 lines per mm slit between 0 and 4000 cm^{-1}.

Water adsorption isotherms were obtained with a Vstar Win instrument (Quantachrome) for water and organic vapors adsorption. Before the determination of the adsorption isotherms, samples were outgassed at 250 °C for 4 h under vacuum.

3. Results and discussion

3.1. Fourier Transform Infrared Spectroscopy (FTIR-ATR)

The as-synthesized polymers were characterized by infrared spectroscopy (Fig. 1). The FTIR-ATR spectrum of polythiophene shows the typical polymer bands. Besides, a broad band around 3400 cm^{-1} that corresponds to O–H stretching shows the presence of adsorbed water on the surface. Two small peaks are distinguished at 3080 and 2916 cm^{-1}, which correspond to the C–H stretching vibration of the ring. At 1675 and 1405 cm^{-1} two peaks, characteristic of C═C asymmetric and symmetric stretching vibration, are shown [63]. The peaks around 1165 and 1040 cm^{-1} correspond to the C–H bending and C–H in-plane deformation respectively. At 790 cm^{-1} a characteristic peak of out-of-plane bending mode of C–H appears, while at 700 cm^{-1} the vibration corresponding to C–S bending is observed, this indicating the presence of sulfur [64].

A broad band between 2000 and 3000 cm^{-1}, corresponding to the O–H stretching of adsorbed water, is observed in the FTIR spectrum of polyaniline. Characteristic peaks of polyaniline appear at lower wavenumbers. The absorption peaks at 1580 and 1490 cm^{-1} are attributed to the C═C stretching vibration of the quinoid and benzenoid rings of

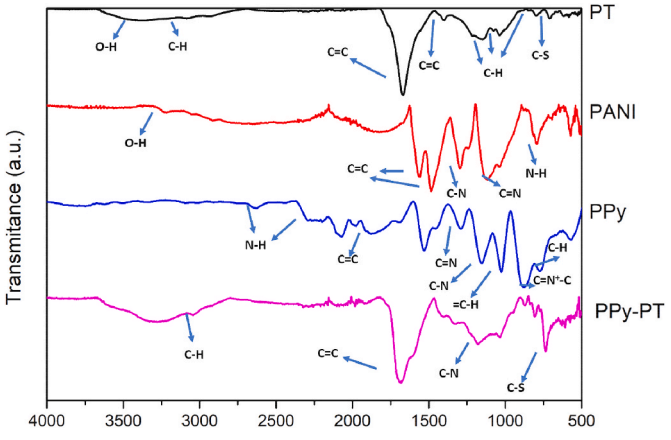

Fig. 1. FTIR-ATR spectra of the synthesized polymers.

emeraldine. The peak which is located at 1250 cm^{-1} is due to the C–N stretching vibration of the secondary amino groups, and the peak at 1190 cm^{-1} is assigned to the C═N stretching mode of the quinoid rings. At 800 cm^{-1} N–H bending appears [65].

In the FTIR spectra of polypyrrole, the absorptions at 2658 and 2324 cm^{-1} are characteristic of the N–H stretching. A peak around 1580 cm^{-1}, due to C═C stretching, can be observed, whereas the peaks at 1300, 1200 and 1050 cm^{-1} correspond to the C═N bending, C–N stretching and =C–H bending vibrations, respectively. The absorptions around 700 and 800 cm^{-1} may be due to out-of-plane vibration of the C–H bond of the polypyrrole ring. The peak at 980 cm^{-1} corresponds to the stretching vibration of the $C{=}N^{+}$-C group [66], which evidences that the oxidized form of polypyrrole has been produced during its synthesis.

The FTIR-ATR spectrum of the polypyrrole-*co*-polythiophene (PPy-PT) copolymer mainly shows the polythiophene bands. A pronounced band corresponding to the bending vibration of the C–S bond over 700 cm^{-1} stands out. However, the C–N stretching band characteristic of polypyrrole can be observed around 1200 cm^{-1}. This suggests that copolymerization of thiophene and pyrrole has occurred, although the contribution of polythiophene units is considerably higher. Consequently, it is ruled out that it is a block copolymer, with blocks of polythiophene and polypyrrole regularly distributed, where the absorptions with similar intensities of both polymers should be appreciated. The spectrum obtained suggests that the chains of polythiophene are considerably longer than those of polypyrrole.

3.2. Thermogravimetric analysis (TGA)

Thermogravimetric analysis (TGA) allows to determine the thermal stability of the pristine polymers, and to predict the carbonization performance at 900 °C (Fig. 2). The thermogravimetric curve of PT shows a weight loss between 80 and 100 °C attributed to the removal of occluded water and/or unreacted monomer. Next, 30 wt% loss in the interval between 200 and 400 °C corresponds to the removal of the counterion dopant of the polymeric chain. From 400 °C there is a linear weight loss due to the polymeric chain breaking and degradation [67]. At 900 °C there is a residue of 30 wt%.

Several stages of weight loss are observed in the PANI thermogravimetric curve. The first loss, approximately 5 wt%, between 25 and 100 °C, is due to the loss of occluded water. Subsequently, three stages of degradation of the polymeric chain centered approximately at 300, 500 and 750 °C are observed [68]. The increase in temperature up to 900 °C originates an additional weight loss, producing a residue of approximately 50 %.

The PPy thermogram shows a 10 wt% loss step between 25 and 150 °C, which corresponds to the loss of volatiles (occluded water, oligomers, and unreacted monomer) [69]. Subsequently, a linear weight loss occurs and a 50 wt% residue is obtained at 900 °C.

The thermogravimetric curve of PPy-PT copolymer shows a loss of occluded water between 50 and 100 °C. The mass loss as a function of temperature then progresses steadily up to 900 °C. This thermogravimetric curve shows similarities with the corresponding curves of PPy and PT polymers. Although the shape of the curve is more similar to that of PT (which is in agreement with the corresponding FTIR-ATR spectra), at 900 °C, a residue of approximately 55 % by mass is obtained, similar to that obtained from PPy, and higher than that obtained with PT (30 %), so it can be deduced that the introduction of PPy units provides thermal stability to PT within the PPy-PT copolymer.

3.2.1. Scanning electron microscopy (SEM)

Once determined, by means of TGA, the weight of the residues obtained after submitting the polymers to a thermal treatment in nitrogen atmosphere from room temperature up to 900 °C, the polymers were pyrolyzed at 900 °C in nitrogen atmosphere to obtain the carbon materials. Subsequently, the obtained carbons were steam activated at 800 °C for 4 h. The surface topography of the carbons was determined by SEM (Fig. 3). The carbons obtained from the pyrolysis of the polymers have a globular morphology with agglomerates of spherical particles. The steam activation treatment does not change the morphology of the carbon materials.

3.3. X-ray photoelectron spectroscopy (XPS)

XPS provides information about the chemical composition of the carbon surface. As expected, nitrogen is detected in the carbons obtained from polyaniline and polypyrrole, although in different amounts depending on the raw polymer (Table 1). Thus, the polyaniline-derived carbon (PANI-P9) shows a nitrogen content of 4.5 at.% versus 1.5 at.% in the polypyrrole-derived carbon (PPy-P9). PANI was synthesized using

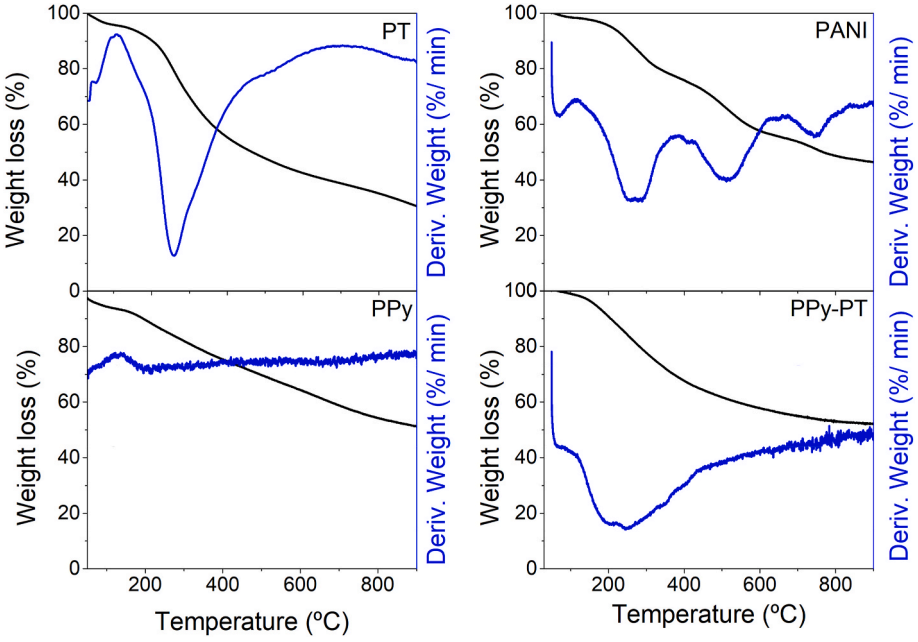

Fig. 2. TGA curves of the synthesized polymers under nitrogen atmosphere.

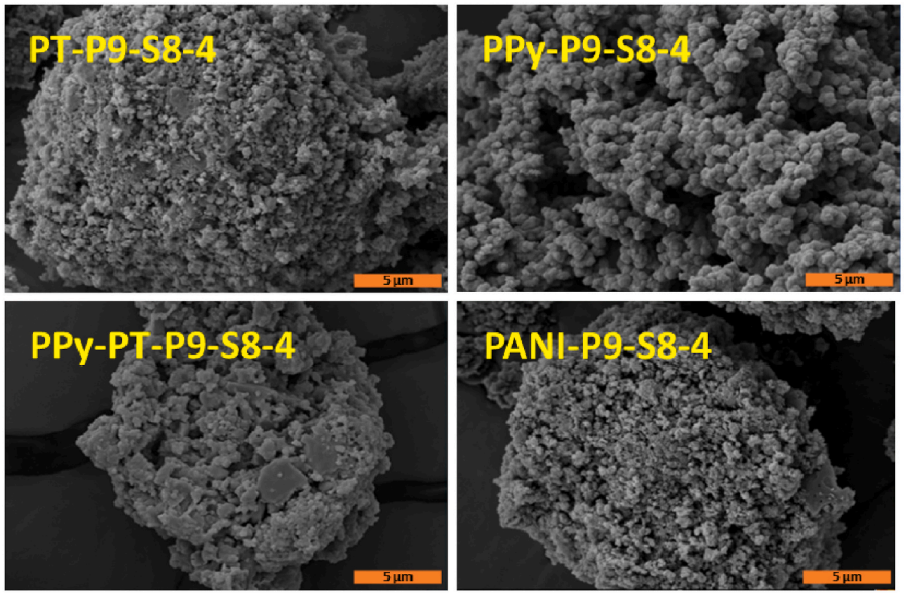

Fig. 3. SEM images of the carbon materials.

Table 1
Surface elemental composition (at.%) of the carbons determined by XPS.

Sample	C 1s	O 1s	S $2p_{3/2}$	N 1s
PT-P9	95.00	2.52	2.48	-
PT-P9-S7-6	95.26	2.50	2.24	-
PT-P9-S8-4	95.51	2.78	1.71	-
PT-P9-S8-6	96.22	2.24	1.54	-
PT-P9-S9-4	96.94	2.08	0.98	-
PANI-P9	92.85	2.70	–	**4.45**
PANI-P9-S8-4	93.89	2.84	–	**3.27**
PPy-P9	90.84	7.63	–	**1.53**
PPy-P9-S8-4	95.19	2.87	–	**1.94**
PPy-PT-P9	85.62	9.98	1.40	**3.00**
PPy-PT-P9-S8-4	91.42	7.23	0.94	**0.41**

sulfuric acid to provide a sulphate counterion to the polymeric chain, however, sulfur is not detected in the carbon obtained from the pyrolysis of PANI.

On the other hand, polythiophene pyrolyzed at 900 °C (PT-P9) gives rise to a carbon with a considerable sulfur amount (2.5 at.%). The carbon obtained from polythiophene after pyrolysis at 900 °C was submitted to a steam activation treatment at three different temperatures (700, 800 and 900 °C). A gradual loss of sulfur is produced as the activation temperature increases, due to the decomposition or reaction of the thermally unstable sulfur species during the activation process [70]. The increase in the steam activation time at 800 °C from 4 to 6 h results in a more important sulfur removal (1.71 at. % in PT-P9-S8-4 vs. 1.54 at. % in PT-P9-S8-6). Despite of the gradual loss of sulfur with the increasing temperature, 1 at.% sulfur is detected at in the carbon steam activated at 900 °C (PT-P9-S9-4). At the activation experimental conditions of 900 °C for 6 h, the carbon was completely burnt out, and no carbon sample remained after the activation process.

Both sulfur and nitrogen are detected in the PPy-PT copolymer, which are partially eliminated during the steam activation. On the other hand, the oxygen atomic percentage oscillates between 2 and 3 at.% in the carbons obtained from PT and PANI but is considerably higher in the PPy-PT copolymer [71].

Curve fit of the high-resolution XPS spectra provides information about the oxidation state, type of bond and chemical environment of each atom. Several nitrogen species can be identified in the high-resolution N 1s spectra. Nitrogen can be present in the form of pyridinic nitrogen (=N–H) (centered at 398.4 eV), pyrrolic (N–H), (centered at 400.0 eV), quaternary -also called graphitic nitrogen- (=N^+-H) centered at 401.7 eV) and pyridinic oxides (N^+-*O*-), centered at 402.1 eV [72–74] (Scheme 1).

Polypyrrole and polyaniline-derived carbons show the contribution of pyridinic nitrogen (=N–H) at ≈398.4 eV, quaternary nitrogen at ≈400.8 eV and oxidized nitrogen at ≈402.2 eV (Fig. 4, Table S2). These nitrogen centers are potentially active for the catalytic reaction, but the relative amount of each species depends on the polymer precursor and the activation treatment. The most abundant species in the polyaniline-derived carbons is the quaternary nitrogen, both in the pyrolyzed polymer (PANI-P9) and in the steam activated polyaniline-derived carbon (PANI-P9-S8-4). In the polypyrrole-derived carbon (PPy-P9), pyridinic and quaternary nitrogen are present on the surface. The activation process (PPy-P9-S8-4) introduces N-oxide species [75]. The carbons prepared from the PPy-PT copolymer show the presence of pyrrolic nitrogen and some contribution of quaternary, which becomes the only species present when this carbon is steam activated. This great variety of nitrogen centers that are potentially active for the catalytic reaction, depend on the nature of polymeric precursor, and also on the pyrolysis and activation conditions.

The deconvolution of the S2p band provides valuable information on the chemical state of the sulfur atoms incorporated into the carbon lattice. 2.5 at.% sulfur is detected in the carbon obtained from polythiophene (PT-P9) (Table 1), showing a single peak around 163.9 eV, which is ascribed to sulfur in C–S–C species (Fig. 5, Table S3). This confirms the incorporation of sulfur to the carbon lattice. Steam activation of this carbon does not modify the nature of the sulfur species. On the other hand, the S2p curve fit corresponding to the carbons obtained from the PPy-PT copolymer, show, in addition to C–S–C species, the contribution to higher binding energy (168.08 eV) of -C-SOx species, which become more important after the steam activation treatment.

3.4. Raman spectroscopy

The carbons microstructure was analyzed by Raman spectroscopy (Figures S1 and S.2. in supporting information). Two main bands, characteristic of activated carbons, are detected. G-band (1580 cm^{-1}), typical of graphite, denotes the crystallinity of the carbon whereas D-band, typical of amorphous carbon (1355 cm^{-1}) is attributed to the

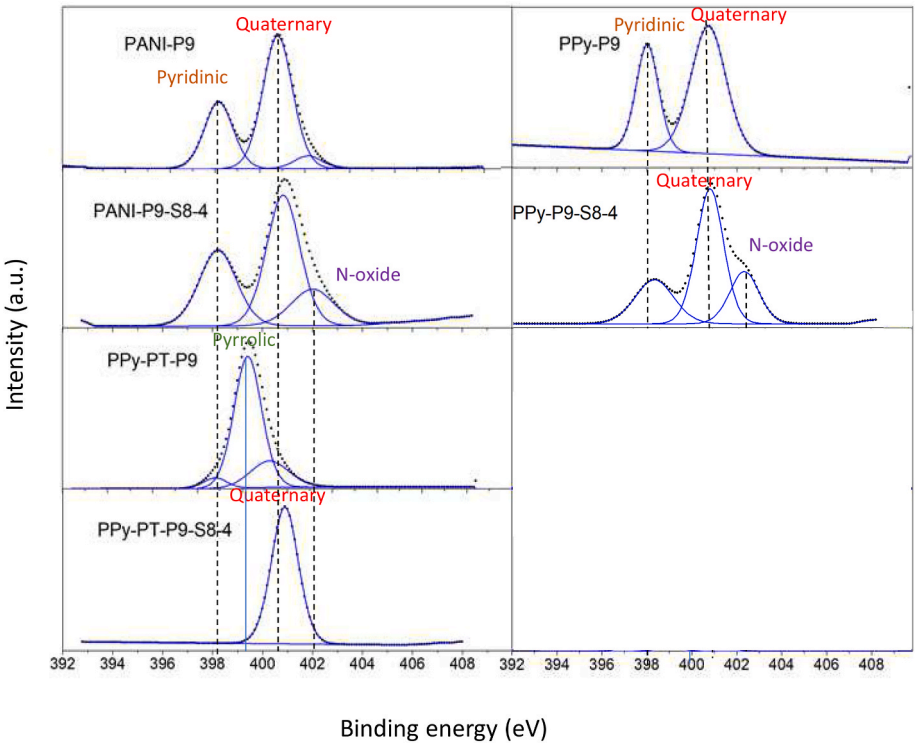

Fig. 4. Curve fit of the high-resolution N 1s XPS spectra.

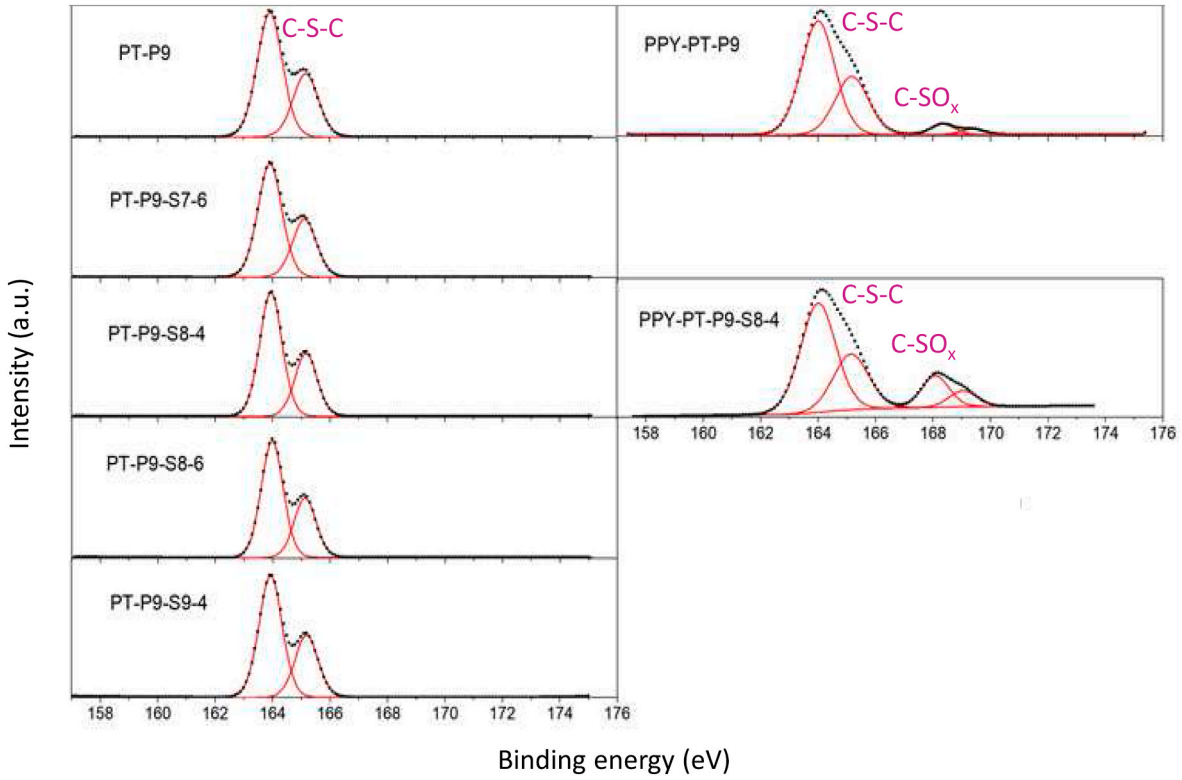

Fig. 5. Curve fit of the high-resolution S 2p XPS spectra.

Table 2
I_D/I_G ratios of the different carbon materials prepared.

Sample	I_D/I_G
PT-P9	1.07
PT-P9-S7-6	1.02
PT-P9-S8-4	1.04
PT-P9-S8-6	1.04
PT-P9-S9-4	1.23
PANI-P9	0.96
PANI-P9-S8-4	0.96
PPy-P9	0.98
PPy-P9-S8-4	0.96
PPy-PT-P9	1.05
PPy-PT-P9-S8-4	0.94

presence of defects and disorder in the structure [76,77]. The ratio between the intensity of these two bands (I_D/I_G) shows the ordering level of the carbon lattice.

The Raman spectra of the carbons obtained from polymers containing nitrogen (PPy and PANI) (Figure S1.) show I_D/I_G ratios between 0.98 and 0.96 (Table 2). These values denote a fairly ordered structure due to the regular chain structure of its polymeric precursors. The pyrolysis of the polymers produces the carbonization of the hydrocarbon chain but not the removal of heteroatoms, which remain anchored to the carbon matrix with a certain degree of order. The activation treatment produces only a slight decrease in the I_D/I_G ratio in the polypyrrole-derived carbon, which can be ascribed to the loss of nitrogen during this process.

The carbons obtained from polythiophene (Figure S2.) show I_D/I_G ratios close to 1, somewhat higher than in the N-containing carbons (Table 2). This can be explained considering that sulfur atoms, which are larger than the carbon atoms, contribute in a great extension to the creation of defects and the consequent increase of the disorder [78]. This is evidenced by the I_D/I_G ratio (1.05) of the N,S-co-doped carbon obtained from polypyrrole-*co*-polytiophene (PPy-PT-P9) due to the defects introduced by S, when it is compared to the I_D/I_G ratio (0.98) of the polypyrrole-derived carbon (PPy-P9). Nevertheless, the highest I_D/I_G ratio (1.23) is observed in the polytiophene-derived carbon steam activated at 900 °C (PT-P9-S9-4), probably due to the higher development of porosity produced during the activation process [79]. Therefore, the carbons textural properties need to be analyzed and quantified.

3.5. N_2 adsorption-desorption isotherms at −196 °C

The textural properties of the carbons were determined by physical adsorption of nitrogen at −196 °C. The corresponding textural parameters have been calculated and are shown in Table 3. The shape of the nitrogen adsorption isotherms of the different carbons obtained from polythiophene is a combination of Type I(a) and Type IV(a) isotherms (Fig. 6a). Type I(a) isotherms are characteristic of microporous solids with narrow micropores (pore size less than 1 nm), while Type IV(a) isotherms present a hysteresis cycle that is due to capillary condensation in mesopores. This confirms the micro-mesoporous nature of the carbons. However, the isotherm of the PT-P9-S9-4 carbon is somewhat different in the low relative pressures range, and it can be classified as Type I(b), which is characteristic of microporous materials with a pore size distribution that covers a broader range, including wider micropores and narrow mesopores. The hysteresis loop observed is of the H1 type, which is associated with “ink-bottle”-shaped pores with a short, narrow neck or cylindrical pores open at both ends.

Table 3
Textural parameters calculated from the adsorption-desorption isotherms of N_2 at −196 °C of the carbons prepared from polythiophene.

Sample	V_{total} (cm^3/g)	V_{micro} (cm^3/g)	V_{meso} (cm^3/g)	S_{BET} (m^2/g)
PT-P9	0.35	0.29	0.06	577
PT-P9-S7-6	0.33	0.27	0.06	548
PT-P9-S8-4	0.44	0.37	0.07	742
PT-P9-S8-6	0.51	0.42	0.09	853
PT-P9-S9-4	0.95	0.63	0.32	1630

The textural parameters obtained from the adsorption isotherms (Table 3) show that the carbon obtained from polythiophene (PT-P9) has a specific surface area of 577 m^2/g, mainly due to the presence of micropores. Activation with steam at 700 °C is not capable of developing porosity (PT-P9-S7-6 has a BET surface of 548 m^2/g). The increase in temperature, as well as in the activation time, results in an increase in the BET surface (742 m^2/g in PT-P9-S8-4 and 853 m^2/g in PT-P9-S8-6). Activation at 900 °C is the most effective in increasing the carbon surface area (1630 m^2/g) due to the development of micro and mesoporosity. This is in agreement with the high I_D/I_G ratio (1.23) observed in the Raman spectrum of PT-P9-S9-4 carbon.

When the carbons obtained from the different polymers are compared (Fig. 6b), it can be concluded that the pyrolysis of polypyrrole at 900 °C produces a non-porous carbon (PPy-P9), being necessary the steam activation of this carbon to create porosity and to increase its surface area. Carbons prepared from polyaniline (PANI-P9), and polytiophene (PT-P9) exhibit a combination of Type I(a) and Type IV(a) isotherms, denoting the presence of micro- and mesoporosity. It is observed that activation with steam at 800 °C for 4 h develops porosity, associated with an increase in the specific surface, which in the case of PT-P9-S8-4 carbon is due to the increase in the volume of micropores, while in PANI-P9-S8-4 and PPy-P9-S8-4 carbons is a consequence of a development of both micro- and mesoporosity (Table 4). These results show that the pyrolysis and steam activation treatments affect each carbon differently, depending on the polymeric precursor used. Under the pyrolysis and activation conditions studied (pyrolysis at 900 °C and steam activation at 800 °C for 4 h), the carbon prepared from polythiophene shows higher specific surface area (742 m^2/g), than that obtained from polyaniline (715 m^2/g), although PANI-P9-S8-4 shows a more developed mesoporosity.

On the other hand, the N, S- co-doped carbon derived from the polypyrrole-*co*-polytiophene copolymer (PPy-PT-P9) exhibits lower surface area and pore volume than its polytiophene-derived carbon counterpart (PT-P9). The introduction of the smaller N heteroatoms, provided by polypyrrole, at the expenses of the larger S atoms, provided by polythiophene produced a decrease of the I_D/I_G ratios from 1.07 in PT-P9 to 1.05 in PPY-PT-P9 (Table 2). However, steam activation treatment produces a development of micro and mesoporosity. As a result, a micro-meso porous N,S-doped activated carbon (PPy-PT-P9-S8-4) with a considerable high BET surface area (893 m^2/g) is obtained.

3.6. CO_2 adsorption-desorption isotherms at 0 °C

A more exhaustive study of microporosity was carried out by comparing the volumes of micropores obtained by adsorption of N_2 at −196 °C and those obtained by adsorption of CO_2 at 0 °C. CO_2 adsorption isotherms at 0 °C are shown in Figure S3 (a) in Supporting information. CO_2 micropore volumes were obtained by applying the Dubining-Raduschkevich (D-R) model to CO_2 adsorption data and were compared with micropore volumes obtained from N_2 adsorption experiments (Table 5). Since the critical dimensions of both molecules are very similar (0.28 nm for CO_2 and 0.30 nm for N_2), the higher adsorption temperature for CO_2 facilitates diffusion through the narrow micropores in which the diffusion of nitrogen molecules is hampered.

It is observed that the isotherms of steam activated carbons at 700 and 800 °C are similar to that of the non-activated carbon, this indicating that activation hardly contributes to the development of porosity in the range of narrow micropores. It stands out the fact that in the sample activated at 900 °C (PT-P9-S9-4) there is even less amount adsorbed, which is in line with the results of N_2 adsorption that showed a widening of the microporosity and the formation of mesopores in this sample. Table 5 shows that V_{micro} (CO_2) > V_{micro} (N_2) values, what is

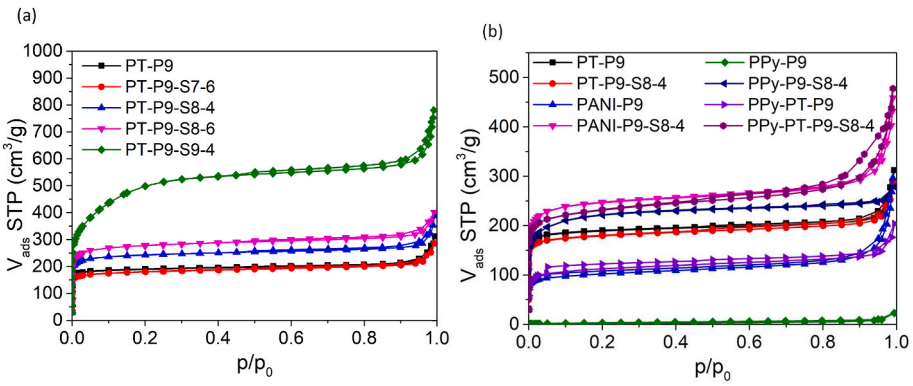

Fig. 6. Nitrogen adsorption-desorption isotherms at −196 °C of carbons prepared from (a) polythiophene; (b) different polymers.

Table 4
Textural parameters calculated from the adsorption-desorption isotherms of N_2 at −196 °C of the carbons prepared from different polymers.

Sample	V_{total} (cm^3/g)	V_{micro} (cm^3/g)	V_{meso} (cm^3/g)	S_{BET} (m^2/g)
PPy-P9	0.01	0.002	0.01	6
PPy-P9-S8-4	0.39	0.33	0.06	648
PANI-P9	0.38	0.27	0.11	302
PANI-P9-S8-4	0.63	0.38	0.25	715
PT-P9	0.35	0.29	0.06	577
PT-P9-S8-4	0.44	0.37	0.07	742
PPy-PT-P9	0.23	0.16	0.01	439
PPy-PT-P9-S8-4	0.56	0.34	0.22	893

Table 5
Micropores volume determined by N_2 and CO_2 adsorption isotherms of carbons prepared from polythiophene.

Sample	V_{micro} (N_2) (cm^3/g)	V_{micro} (CO_2) (cm^3/g)
PT-P9	0.29	0.33
PT-P9-S7-6	0.27	0.31
PT-P9-S8-4	0.37	0.37
PT-P9-S8-6	0.42	0.36
PT-P9-S9-4	0.60	0.33

indicative of very narrow microporosity in the non-activated carbon (PT-P9) and in the carbon activated at 700 °C (PT-P9-S7-6). As the steam activation temperature increases, this relationship inverts, so that V_{micro} (CO_2) < V_{micro} (N_2), which is indicative of a broader micropore size distribution. Consequently, activation with steam at elevated temperatures contributes to microporosity widening.

When the carbons obtained from the different polymers are compared (Figure S3 (b) in Supporting information), the lack of porosity of the carbon from polypyrrole before being activated (PPy-P9) stands out. Steam activation at 800 °C for 4 h notably increases its microporosity. This is in line with the conclusions extracted from the study of the N_2 adsorption isotherms (Fig. 6).

Table 6
Micropore volume determined by N_2 and CO_2 adsorption isotherms of the carbons derived from the different polymeric precursors.

Sample	V_{micro} (N_2) (cm^3/g)	V_{micro} (CO_2) (cm^3/g)
PT-P9	0.29	0.33
PT-P9-S8-4	0.37	0.37
PANI-P9	0.27	0.23
PANI-P9-S8-4	0.38	0.30
PPy-P9	0.00	0.00
PPy-P9-S8-4	0.33	0.24
PPy-PT-P9	0.16	0.26
PPy-PT-P9-S8-4	0.34	0.33

Regarding the copolymer-derived carbons, the CO_2 adsorption isotherms of PPy-PT-P9 and PPy-PT-P9-S8-4 are more similar to those of the polythiophene derived-carbons (PT-P9 and PT-P9-S8-4) (Figure S3.) than those of the polypyrrole-derived carbons (PPy-P9 and PPy-P9-S8-4). These findings evidence that the textural properties of the resulting N,P-co-doped carbon are mainly determined by the presence in the carbon precursor of S provided by polythiophene, rather than N provided by polypyrrole. Besides, V_{micro} (CO_2) < V_{micro} (N_2) value in PPy-PT-P9-S8-4 (Table 6) confirms that the steam activation develops a broad micropore size distribution in this carbon, as well as develops mesoporosity, as evidenced by N_2 adsorption measurements. This developed micro-mesoporosity contribute to the high BET surface area (893 m^2/g) of the steam activated N,S-co-doped-carbon (Table 4).

On the other hand, contrary to what was observed in the S.doped carbons, there is not a remarkable broadening of the micropores produced by the steam activation in PPy-P9-S8-4 and PANI-P9-S8-4 carbons, as it is evidenced from the small difference between V_{micro} (CO_2) and V_{micro} (N_2) values (Table 6).

3.7. Water adsorption-desorption isotherms at 25 °C

Depending on the specific application of a given activated carbon, its water adsorption capacity can be considered as a problem or as a desired characteristic. Thus, it is a problem when trying to remove volatile organic compounds (VOC) such as benzene or toluene from gas streams, since the adsorption of these compounds by activated carbon can be hindered by the presence of water. On the other hand, the water adsorption capacity of carbon is desirable for other applications, such as those related to adsorption heat pumps. Although the surface of activated carbons is inherently hydrophobic, some studies [80,81] report that the presence of O and N containing-functional groups, together with the presence of defects, can favor the adsorption of water at low humidity, since they act as anchoring sites for water molecules. In this sense, the adsorption of water at low humidity (or low relative pressure) can be used as an indication of the amount of surface functional groups in activated carbons.

The adsorption-desorption isotherms of water at 25 °C on the carbons obtained from polythiophene (Fig. 7a) can be classified as Type V, where adsorption occurs at high relative pressures due to a weak interaction between the adsorbate and the adsorbent. The samples with the highest sulfur content (determined by XPS, Table 1), which are those activated at lower temperatures (PT-P9-S7-6), show a greater adsorption of water vapor at low relative pressures. These results suggest that sulfur functionalities act as anchoring centers for water molecules. A strong dependence of the shape of the water adsorption-desorption isotherms on the activation temperature is also observed, which is related to the type of porosity developed at each temperature. A widening of the hysteresis loop is observed as the temperature and activation time increase. This is due to a development of porosity that favors the packing

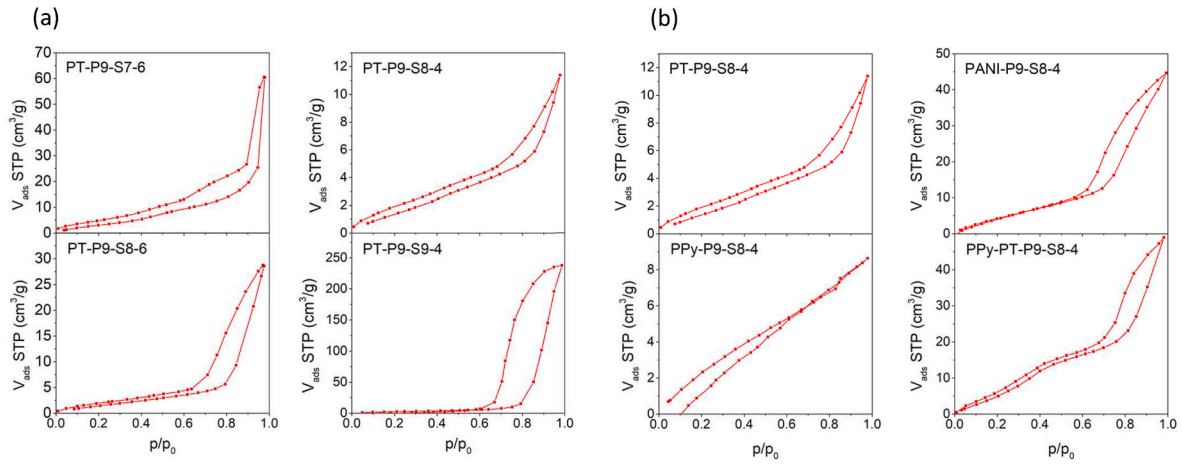

Fig. 7. Water adsorption-desorption isotherms at 25 °C of the carbons prepared from (a) polythiophene; (b) different polymers.

of adsorbed water molecules [82]. Consequently, PT-P9-S9-4 carbon shows an important water adsorption capacity at high relative pressures, as a consequence of its well-developed porosity. In addition, the presence of sulfur atoms from polythiophene enhances adsorption at low relative pressures, even in carbons activated at high temperatures, where the S content is lower than those activated at low temperatures.

It has been reported [82–84] that the adsorption of water at low pressures is due to the presence of surface groups, while the adsorption at high pressures is favored by the presence of a high volume of pores. The desorption mechanism is different depending on the type of porosity present in the activated carbon. When not properly developed, water adsorption is primarily determined by the number of active sites to which water molecules can attach. If the activated carbons have a well-developed porosity, the initial growth of clusters of water molecules is favored, which can be packed in the pores more effectively. It has been observed that at high relative pressures (>0.5), the adsorption of water is determined by the development of porosity, which favors the packing of water molecules as three-dimensional clusters. Consequently, the best adsorption capacity of water is shown by PT-P9-S9-4 carbon, which has been activated at 900 °C, despite its lower sulfur content (0.98 at.%, determined by XPS; Table 1).

The water vapor adsorption capacity of the carbons prepared from the different polymers or copolymers at the same experimental conditions of pyrolysis (900 °C) and activation experimental conditions (800 °C, 4 h) is different depending on the polymeric precursors of the carbon and its different content in heteroatoms (Fig. 7b). It draws the attention that, together with a low water adsorption produced on the polypyrrole-derived carbon (PPy-P9-S8-4), the hysteresis loop between the adsorption and desorption branches of the isotherm fail to close, which may be due to the presence of very narrow porosity that causes adsorbed water to be occluded inside the pores.

Regarding the copolymer-derived carbon, it can be observed that the isotherm corresponding to the polypyrrole-*co*-polythiophene-derived carbon (PPy-PT-P9-S8-4) is similar in shape to that of its counterpart obtained exclusively from polythiophene (PT-P9-S8-4), except for the widening of the hysteresis cycle and the considerable increase in the volume of water adsorbed at high relative pressures observed in the carbon obtained from the copolymer (PPy-PT-P9-S8-4). These results evidence the enhanced water adsorption capacity of this N,S co-doped carbon, compared to the S-doped carbon obtained exclusively from polytiophene (PT-P9-S8-4) or the N-doped carbon obtained from polypyrrole (PPy-P9-S8- 4).

3.8. Catalytic test

The catalytic activity of the carbons prepared from the different polymers has been evaluated in the hydrogenation reaction of 1-chloro-4-nitrobenzene. All the metal-free carbons are active in the reaction, with a selectivity of 100 % towards the hydrogenation of the nitro group.

The carbon prepared from the pyrolysis of polythiophene (PT-P9) provides 50 % conversion after 1400 min of reaction (Fig. 8a). Steam activation does not improve these features, except for PT-P9-S8-4 carbon, where a final conversion of 80 % is obtained. This degree of conversion (with a selectivity of 100 % towards the nitro group) is similar to that obtained by Liu and Chen [85] using a nickel catalyst. However, in this work it has not been necessary to use metallic particles, and are the functional groups of the activated carbon that act as catalytic sites. The results show that the carbon activated at 800 °C for 4 h maintains a

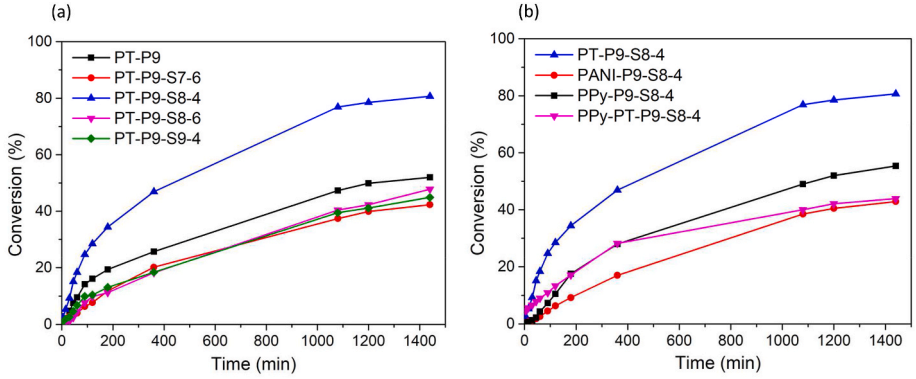

Fig. 8. Catalytic test of the carbons prepared from (a) polythiophene; (b) different polymers.

compromise between adequate textural characteristics, with S_{BET} = 742 m^2/g, V_{micro} (N_2) = 0.37 cm^3/g, V_{micro} (CO_2) = 0.37 cm^3/g and V_{meso} (N_2) = 0.07 cm^3/g, without considerable loss of sulfur (1.71 at.%, analyzed by XPS) produced by the steam activation treatment. Activation treatments under more extreme conditions, although resulting in developed porosity, they also give rise to the loss of a large part of the surface sulfur, with a consequent decrease in catalytic activity. A compromise between sulfur doping level and porosity is therefore necessary.

There is much controversy about which species are active for the hydrogenation of nitroarenes. XPS spectra of N-doped steam-activated carbons derived from polyaniline (PANI-P9-S8-4) and from polypyrrole (PPy-P9-S8-4) showed quaternary nitrogen as the predominant species, although pyridinic and N-oxide were also present (Fig. 4). N,S-codoped carbon obtained from the polypyrrole-*co*-polytiophene copolymer (PPy-PT-P9-S8-4), exhibited quaternary-N species and C–S–C and C-SO_x sulfur functionalities. This N,S-codoped carbon, with just 0.4 at% N and 0.9 at% S shows a catalytic performance (Fig. 8b) similar to that of the N-doped carbon (PPy-P9-S8-4) with a nitrogen content five times higher (2.0 at.% N).

What is more, the highest degree of conversion (Fig. 8b) is obtained with the S-doped steam-activated carbon (PT-P9-S8-4) with a sulfur content of 1.71 at. % in the form of C–S–C species. As this carbon lacks of nitrogen, these data suggest that sulfur is more active than nitrogen in the hydrogenation reaction of 1-chloro-4-nitrobenzene. Raman spectroscopy evidenced the increased desorder produced by the introduction of sulfur into the carbon lattice. Based on the analysis of XPS and Raman spectra, it can be concluded that the formation of defects resulting from S doping is determinant to achieve a high catalytic performance.

The reusability of PT-P9-S8-4 carbon was tested in the hydrogenation reaction of 1-chloro-4-nitrobenzene for 5 consecutive cycles. Although a gradual decrease of conversion was produced with the reuse (Fig. 9), probably due to a partial inactivation of the catalyst and a reduced accessibility to the active sites, conversion above 70 % was still achieved during the 5th cycle after 1440 min. Selectivity was not affected and a 100 % selectivity towards the hydrogenation of the nitro group was always achieved.

Heteroatom doping [86] effectively facilitates adsorption and activation of H_2 and the nitro group and lowers the energy barrier of the aniline-producing process. The introduction of heteroatoms (even at a low level) can effectively change the electronic configuration of the carbon atom near the dopant atom [42,87]. The combination of the heteroatom dopant and the lattice defect in carbon can cause significant electron delocalization and thus both H_2 and the nitro (-NO_2) group are easily activated for selective hydrogenation. Therefore, the search for a suitable catalyst for the hydrogenation of 1-chloro-4-nitrobenzene with adequate catalytic activity, high selectivity and stability relies on a tunable concentration of dopant heteroatom, lattice defects and developed porosity, which favors the access of the reactants to the catalytic sites.

In this work it has been demonstrated that the degree of conversion achieved in the hydrogenation of 1-chloro-4-nitrobenzene, catalyzed by metal-free doped activated carbons relies on, an adequate porosity of the activated carbon, which is determined by the steam activation conditions, and also on the presence of heteroatoms that act as active catalytic sites. In this respect it has been demonstrated that S sites are more active than N. Thus, the main active sites are located at defects produced by the introduction of S in the carbon lattice. A plausible mechanism for the hydrogenation of 1-chloro-4-nitrobenzene must consider not only C, N and S relative sizes, but also the electronegativity difference between the doping atoms and C. Therefore, H_2 adsorbed on the carbon surface would be activated at the N and S active sites. The resulting species produced after the heterolytic cleavage of H_2 ($H^{\delta+}$ and $H^{\delta-}$) would bond to the doped carbon producing either N-$H^{\delta+}$ or S-$H^{\delta+}$, and C-$H^{\delta-}$. Then, 1-chloro-4-nitrobenzene, would be reduced with the assistance of these species. As S is adsorbed preferably at the defects, the closer proximity of S-$H^{\delta+}$ to the adsorbed nitrobenzene would enhance the catalytic performance of the S-doped activated carbons.

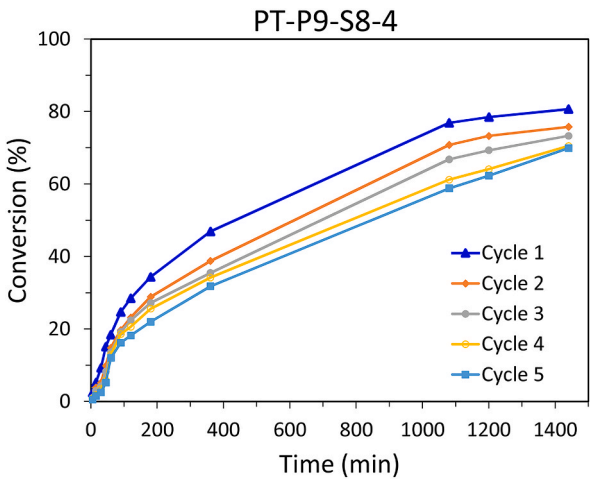

Fig. 9. Cyclic experiments showing the reusability of PT-P9-S8-4 carbon in the hydrogenation reaction of 1-chloro-4-nitrobenzene.

4. Conclusions

In this work, sulfur-doped carbons have been prepared from polythiophene, a sulfur containing polymer. The influence of the activation conditions on the porous properties of the prepared materials and on their surface chemistry has been evaluated, and their activity as metal-free catalysts in the hydrogenation reaction of 1-chloro-4-nitrobenzene has been determined. The chemical and physical properties, as well as the catalytic performance of the sulfur-doped carbons have been compared with those of nitrogen-doped carbons prepared from nitrogen-containing polymers (polyaniline and polypyrrole).

The following conclusions can be extracted from the obtained experimental results.

1. All the metal-free carbon materials prepared are active in the hydrogenation reaction of 1-chloro-4-nitrobenzene, with a selectivity of 100 %. The degree of conversion in the reaction depends on the development of an adequate porosity in the activated carbon (which is determined by the activation conditions) together with the presence of heteroatoms that act as active catalytic sites. In this study, it has been demonstrated that sulfur doping is considerably more effective than nitrogen in enhancing the catalytic activity of the activated carbons.
2. The increased temperature and time of the steam activation allows to develop the porosity of the carbon but produces a loss of surface sulfur. Therefore, a compromise between an acceptable level of doping with sulfur and the development of adequate porosity is crucial for maximizing the catalytic performance of these materials. This balance has been achieved in a carbon obtained from polythiophene pyrolyzed at 900 °C and steam activated at 800 °C for 4 h.

The importance of tailored activation and heteroatom doping in producing effective catalysts for the hydrogenation of 1-chloro-4-nitrobenzene has been demonstrated.

Author contributions

The manuscript was written through contributions of all authors. All authors have given approval to the final version of the manuscript.

Declaration of competing interest

The authors declare that they have no known competing financial interests or personal relationships that could have appeared to influence the work reported in this paper.

Acknowledgment

Financial support from Spain Ministry of Science and Innovation (PID2019-108453GB-C21) is gratefully acknowledged.

Appendix A. Supplementary data

Supplementary data to this article can be found online at https://doi.org/10.1016/j.ijhydene.2023.12.005.

References

[1] Kovacic P, Somanathan R. Nitroaromatic compounds: environmental toxicity, carcinogenicity, mutagenicity, therapy and mechanism. J Appl Toxicol 2014;34(8):810–24.
[2] Song J, Huang ZF, Pan L, Li K, Zhang X, Wang L, Zou JJ. Review on selective hydrogenation of nitroarene by catalytic, photocatalytic and electrocatalytic reactions. Appl Catal, B 2018;227:386–408.
[3] Du JT, Qiao M, Pu Y, Wang JX, Chen JF. Aqueous dispersions of monodisperse Pt, Pd, and Au nanoparticles stabilized by thermosensitive polymer for the efficient reduction of nitroarenes. Appl Catal Gen 2021;624:118323.
[4] Kadam HK, Tilve SG. Advancement in methodologies for reduction of nitroarenes. RSC Adv 2015;5(101):83391–407.
[5] Eppinger J, Huang KW. Formic acid as a hydrogen energy carrier. ACS Energy Lett 2017;2:188–95.
[6] Saka C. Efficient and durable H2 production from NaBH4 methanolysis using N doped hybrid G-C_3N_4-SiO_2 composites with ammonia as a nitrogen source. Fuel 2022;324:124594.
[7] Sahoo B, Formenti D, Topf C, Bachmann S, Scalone M, Junge K, Beller M. Biomass-derived catalysts for selective hydrogenation of nitroarenes. ChemSusChem 2017;10(15):3035–9.
[8] Sheng Y, Wu B, Ren J, Wang X, Zou X, Lu X. Efficient and recyclable bimetallic Co–Cu catalysts for selective hydrogenation of halogenated nitroarenes. J Alloys Compd 2022;897:163143.
[9] Lara P, Philippot K. The hydrogenation of nitroarenes mediated by platinum nanoparticles: an overview. Catal Sci Technol 2014;4(8):2445–65.
[10] Song J, Huang ZF, Pan L, Li K, Zhang X, Wang L, Zou JJ. Review on selective hydrogenation of nitroarene by catalytic, photocatalytic and electrocatalytic reactions. Appl Catal, B 2018;227:386–408.
[11] Hu ZN, Liang J, Ding K, Ai Y, Liang Q, Sun H bin. Insight into the selectivity of nano-catalytic nitroarenes reduction over other active groups by exploring hydrogen sources and metal components. Appl Catal Gen 2021;626:118339.
[12] Movahed SK, Jafari P, Mallakpour S. Ruthenium nickel bimetallic nanoparticles embedded in nitrogen-doped carbon mesoporous spheres as a superior catalyst for the hydrogenation of toxic nitroarenes. J Environ Chem Eng 2023;11:110426.
[13] Nie R, Wang J, Wang L, Qin Y, Chen P, Hou Z. Platinum supported on reduced graphene oxide as a catalyst for hydrogenation of nitroarenes. Carbon 2012;50(2):586–96.
[14] Chen M, Zhang M, Liu X, Liu Y. Pt/C-Catalyzed selective hydrogenation of nitroarenes to N-arylhydroxylamines under mild conditions. ChemistrySelect 2023;8:1–6.
[15] Zhang Y, Zhou J. Synergistic catalysis by a hybrid nanostructure Pt catalyst for high-efficiency selective hydrogenation of nitroarenes. J Catal 2021;395:445–56.
[16] Mohammadi P, Heravi MM, Mohammadi L, Saljooqi A. Preparation of magnetic biochar functionalized by polyvinyl imidazole and palladium nanoparticles for the catalysis of nitroarenes hydrogenation and sonogashira reaction. Sci Rep 2023;13:17375.
[17] Zhang S, Chang CR, Huang ZQ, Li J, Wu Z, Ma Y, Zhang Z, Wang Y, Qu Y. High catalytic activity and chemoselectivity of sub-nanometric Pd clusters on porous nanorods of CeO_2 for hydrogenation of nitroarenes. J Am Chem Soc 2016;138(8):2629–37.
[18] Zhang J, Wang L, Shao Y, Wang Y, Gates BC, Xiao FS. A Pd@zeolite catalyst for nitroarene hydrogenation with high product selectivity by sterically controlled adsorption in the zeolite micropores. Angew Chem Int Ed 2017;129(33):9879–83.
[19] Zuo LJ, Xue KZ, Xu SL, Kong Y, Liang HW. Intermetallic Rh_3Sn_2 catalysts for selective hydrogenation of functionalized nitroarenes to aromatic ammonia. ChemCatChem 2023;15:1–6.
[20] K N, Ravindra PA, B A, Kannan N, G P, Sinha A. Highly efficient phosphine-free half-sandwich ruthenium(II) catalysts for hydrogenation of nitroarenes. J Mol Struct 2023;1294:136302.
[21] Gao R, Pan L, Lu J, Xu J, Zhang X, Wang L, Zou JJ. Phosphorus-doped and lattice-defective carbon as metal-like catalyst for the selective hydrogenation of nitroarenes. ChemCatChem 2017;9(22):4287–94.
[22] Liu X, Wang C, Meng J, Yue X, Wang Q, Lu J, Wang J, Wang X, Zong Y, Jiang X. Single-atom cobalt catalysts for chemoselective hydrogenation of nitroarenes to anilines. Chin Chem Lett 2023;34:108745.
[23] Zhuang X, Jin K, Zhang Q, Liu J, Zhang X, Zhan H, Ma L. One-pot synthesis of Fe_xO_y nanoparticles embedded within N-doped carbon layers as highly efficient and selective catalysts for the hydrogenation of nitroarenes. Chin Chem Lett 2023;34:107954.
[24] Li Z, Chen Y, Ji S, Tang Y, Chen W, Li A, Zhao J, Xiong Y, Wu Y, Gong Y, Yao T, Liu W, Zheng L, Dong J, Wang Y, Zhuang Z, Xing W, He CT, Peng C, Cheong WC, Li Q, Zhang M, Chen Z, Fu N, Gao X, Zhu W, Wan J, Zhang J, Gu L, Wei S, Hu P, Luo J, Li J, Chen C, Peng Q, Duan X, Huang Y, Chen XM, Wang D, Li Y. Iridium single-atom catalyst on nitrogen-doped carbon for formic acid oxidation synthesized using a general host–guest strategy. Nat Chem 2020;12(8):764–72.
[25] Li B, Li H, Wang N, Sun X, Gao X, Chen J, Wang X, Chang H, Song D, Li J. Ultrasmall Ru nanoparticles highly dispersed on sulfur-doped graphene for HER with high electrocatalytic performance. ACS Appl Mater Interfaces 2020;12(43):48591–7.
[26] Yuan Z, Liu B, Zhou P, Zhang Z, Chi Q. Preparation of nitrogen-doped carbon supported cobalt catalysts and its application in the reductive amination. J Catal 2019;370:347–56.
[27] Varela AS, Ju W, Bagger A, Franco P, Rossmeisl J, Strasser P. Electrochemical reduction of CO_2 on metal-nitrogen-doped carbon catalysts. ACS Catal 2019;9(8):7270–84.
[28] Jarrais B, Guedes A, Freire C. Heteroatom-doped carbon nanomaterials as metal-free catalysts for the reduction of 4-nitrophenol. ChemistrySelect 2018;3(6):1737–48.
[29] Li G, Zheng S, Wang L, Zhang X. Metal-free chemoselective hydrogenation of nitroarenes by N-doped carbon nanotubes via in situ polymerization of pyrrole. ACS Omega 2020;5(13):7519–28.
[30] Hu X, Fan M, Zhu Y, Zhu Q, Song Q, Dong Z. Biomass-derived phosphorus-doped carbon materials as efficient metal-free catalysts for selective aerobic oxidation of alcohols. Green Chem 2019;21:5274–83.
[31] Huo J, Duan P, Pham HN, Chan YJ, Datye AK, Schmidt-Rohr K, Shanks BH. Improved hydrothermal stability of Pd nanoparticles on nitrogen-doped carbon supports. Catal Sci Technol 2018;8(14):3548–61.
[32] Chen H, Sun F, Wang J, Li W, Qiao W, Ling L, Long D. Nitrogen doping effects on the physical and chemical properties of mesoporous carbons. J Phys Chem C 2013;117(16):8318–28.
[33] Luo Z, Lim S, Tian Z, Shang J, Lai L, MacDonald B, Fu C, Shen Z, Yu T, Lin J. Pyridinic N doped graphene: synthesis, electronic structure, and electrocatalytic property. J Mater Chem 2011;21(22):8038–44.
[34] Quílez-Bermejo J, Morallón E, Cazorla-Amorós D. Metal-free heteroatom-doped carbon-based catalysts for ORR. A critical assessment about the role of heteroatoms. Carbon 2020;165:434–54.
[35] Saka C. Very efficient dehydrogenation of methanolysis reaction with nitrogen doped chlorella vulgaris microalgae carbon as metal-free catalysts. Int J Hydrogen Energy 2021;46:20961–71.
[36] Paraknowitsch JP, Thomas A. Doping carbons beyond nitrogen: an overview of advanced heteroatom doped carbons with boron, sulphur and phosphorus for energy applications. Energy Environ Sci 2013;6(10):2839–55.
[37] Bosilj M, Rustam L, Thomann R, Melke J, Fischer A, White RJ. Directing nitrogen-doped carbon support chemistry for improved aqueous phase hydrogenation catalysis. Catal Sci Technol 2020;10(14):4794–808.
[38] Kang KY, Lee BI, Lee JS. Hydrogen adsorption on nitrogen-doped carbon xerogels. Carbon 2009;47(4):1171–80.
[39] Saka C. Highly active and durable hydrogen release in $NaBH_4$ methanolysis reaction with sulphur and phosphorus-doped metal-free microalgal carbon nanoparticles. Appl Catal, B 2021;292:120165.
[40] Chacón FJ, Cayuela ML, Roig A, Sánchez-Monedero MA. Understanding, measuring and tuning the electrochemical properties of biochar for environmental applications. Rev Environ Sci Biotechnol 2017;16(4):695–715.
[41] Saka C. Oxygen and nitrogen-doped metal-free microalgae carbon nanoparticles for efficient hydrogen production from sodium borohydride in methanol. Int J Hydrogen Energy 2021;46:26298–307.
[42] Hu X, Sun X, Song Q, Zhu Y, Long Y, Dong ZN. S Co-doped hierarchically porous carbon materials for efficient metal-free catalysis. Green Chem 2020;22:742–52.
[43] Saka C. Surface modification of graphitic carbon nitride nanoparticles with B, O and S doping/carbon vacancy for efficient dehydrogenation of sodium borohydride in methanol. Int J Hydrogen Energy 2023;48:13123–38.
[44] Seredych M, László K, Bandosz TJ. Sulfur-doped carbon aerogel as a metal-free oxygen reduction catalyst. ChemCatChem 2015;7(18):2924–31.
[45] Liu S, Cui L, Peng Z, Wang J, Hu Y, Yu A, Wang H, Peng P, Li FF. Eco-friendly synthesis of N,S Co-doped hierarchical nanocarbon as a highly efficient metal-free catalyst for the reduction of nitroarenes. Nanoscale 2018;10(46):21764–71.
[46] Yang Z, Yao Z, Li G, Fang G, Nie H, Liu Z, Zhou X, Chen X, Huang S. Sulfur-doped graphene as an efficient metal-free cathode catalyst for oxygen reduction. ACS Nano 2012;6(1):205–11.
[47] Hasegawa G, Deguchi T, Kanamori K, Kobayashi Y, Kageyama H, Abe T, Nakanishi K. High-level doping of nitrogen, phosphorus, and sulfur into activated carbon monoliths and their electrochemical capacitances. Chem Mater 2015;27(13):4703–12.
[48] Shan J, Sun X, Zheng S, Wang T, Zhang X, Li G. Graphitic N-dominated nitrogen-doped carbon nanotubes as efficient metal-free catalysts for hydrogenation of nitroarenes. Carbon 2019;146:60–9.

[49] Gao Y, Hu G, Zhong J, Shi Z, Zhu Y, Su DS, Wang J, Bao X, Ma D. Nitrogen-doped sp^2-hybridized carbon as a superior catalyst for selective oxidation. Angew Chem Int Ed 2013;52(7):2109–13.
[50] Xiong W, Wang Z, He S, Hao F, Yang Y, Lv Y, Zhang W, Liu P, Luo H. Nitrogen-doped carbon nanotubes as a highly active metal-free catalyst for nitrobenzene hydrogenation. Appl Catal, B 2020;260:118105.
[51] Kiciński W, Dziura A. Heteroatom-doped carbon gels from phenols and heterocyclic aldehydes: sulfur-doped carbon xerogels. Carbon 2014;75:56–67.
[52] Wang H, Bo X, Zhang Y, Guo L. Sulfur-doped ordered mesoporous carbon with high electrocatalytic activity for oxygen reduction. Electrochim Acta 2013;108:404–11.
[53] Zhu J, Chen R, Zeng Z, Su C, Zhou K, Mo Y, Guo Y, Zhou F, Gao J, Li L. Acetone adsorption capacity of sulfur-doped microporous activated carbons prepared from polythiophene. Environ Sci Pollut Res 2019;26(16):16166–80.
[54] Xia Y, Zhu Y, Tang Y. Preparation of sulfur-doped microporous carbons for the storage of hydrogen and carbon dioxide. Carbon 2012;50(15):5543–53.
[55] Brédas JL, Elsenbaumer RL, Chance RR, Silbey R. Electronic properties of sulfur containing conjugated polymers. J Chem Phys 1983;78(9):5656–62.
[56] Gök A, Omastová M, Yavuz AG. Synthesis and characterization of polythiophenes prepared in the presence of surfactants. Synth Met 2007;157(1):23–9.
[57] Karim MR, Lee CJ, Lee MS. Synthesis and characterization of conducting polythiophene/carbon nanotubes composites. J Polym Sci Polym Chem 2006;44 (18):5283–90.
[58] García-Fernández MJ, Sancho-Querol S, Pastor-Blas MM, Sepúlveda-Escribano A. Surfactant-assisted synthesis of conducting polymers. Application to the removal of nitrates from water. J Colloid Interface Sci 2017;494:98–106.
[59] Anfar Z, El Fakir AA, Zbair M, Hafidi Z, Amedlous A, Majdoub M, Farsad S, Amjlef A, Jada A, El Alem N. New functionalization approach synthesis of sulfur doped, nitrogen doped and Co-doped porous carbon: superior metal-free carbocatalyst for the catalytic oxidation of aqueous organics pollutants. Chem Eng J 2021;405:126660.
[60] Wang Z, Su R, Wang D, Shi J, Wang JX, Pu Y, Chen JF. Sulfurized graphene as efficient metal-free catalysts for reduction of 4-nitrophenol to 4-aminophenol. Ind Eng Chem Res 2017;56(46):13610–7.
[61] García-Fernández MJ, Buitrago-Sierra R, Pastor-Blas MM, Soares OSGP, Pereira MFR, Sepúlveda-Escribano A. Green synthesis of polypyrrole-supported metal catalysts: application to nitrate removal in water. RSC Adv 2015;5(41): 32706–13.
[62] García-Fernández MJ, Pastor-Blas MM, Epron F, Sepúlveda-Escribano A. Proposed mechanisms for the removal of nitrate from water by platinum catalysts supported on polyaniline and polypyrrole. Appl Catal, B 2018;225:162–71.
[63] Kausar A. Synthesis and electrical property of polythiophene/sol-gel silver nanoparticle-based polyethylene composite. Int J Compos Mater 2016;6(2):43–7.
[64] Senthilkumar B, Thenamirtham P, Kalai Selvan R. Structural and electrochemical properties of polythiophene. Appl Surf Sci 2011;257(21):9063–7.
[65] Gholami H, Shakeri A, Saadattalab V. Investigation of physical and mechanical properties of polyaniline/MMT nanocomposites. Current Chemistry Letters 2017;6 (4):151–8.
[66] Ahmad S, Khan I, Husain A, Khan A, Asiri AM. Electrical conductivity based ammonia sensing properties of polypyrrole/MoS_2 nanocomposite. Polymers 2020; 12(12):1–13.
[67] Mohammad F, Calvert PD, Billingham NC. Thermal stability of electrochemically prepared polythiophene and polypyrrole. Bull Mater Sci 1995;18(3):255–61.
[68] Alves WF, Venancio EC, Leite FL, Kanda DHF, Malmonge LF, Malmonge JA, Mattoso LHC. Thermo-analyses of polyaniline and its derivatives. Thermochim Acta 2010;502(1–2):43–6.
[69] Ramesan MT. Synthesis, characterization, and conductivity studies of polypyrrole/copper sulfide nanocomposites. J Appl Polym Sci 2013;128(3):1540–6.
[70] Wang EJ, Sui ZY, Sun YN, Ma Z, Han BH. Effect of porosity parameters and surface chemistry on carbon dioxide adsorption in sulfur-doped porous carbons. Langmuir 2018;34(22):6358–66.
[71] Sevilla M, Fuertes AB. Highly porous S-doped carbons. Microporous Mesoporous Mater 2012;158:318–23.
[72] Ejaz A, Jeon S. The individual role of pyrrolic, pyridinic and graphitic nitrogen in the growth kinetics of Pd NPs on N-rgo followed by a comprehensive study on ORR. Int J Hydrogen Energy 2018;43(11):5690–702.
[73] Liu P, Gao S, Wang Y, Huang Y, He W, Huang W, Luo J. Carbon nanocages with N-doped carbon inner shell and Co/N-doped carbon outer shell as electromagnetic wave absorption materials. Chem Eng J 2020;381:122653.
[74] Ferrero GA, Sevilla M, Fuertes AB. Mesoporous carbons synthesized by direct carbonization of citrate salts for use as high-performance capacitors. Carbon 2015; 88:239–51.
[75] Duan X, Sun H, Wang Y, Kang J, Wang S. N-Doping-Induced nonradical reaction on single-walled carbon nanotubes for catalytic phenol oxidation. ACS Catal 2015;5 (2):553–9.
[76] Shimodaira N, Masui A. Raman spectroscopic investigations of activated carbon materials. J Appl Phys 2002;92(2):902–9.
[77] Lee AY, Yang K, Anh ND, Park C, Lee SM, Lee TG, Jeong MS. Raman study of D* band in graphene oxide and its correlation with reduction. Appl Surf Sci 2021;536: 147990.
[78] Sun Y, Wu J, Tian J, Jin C, Yang R. Sulfur-doped carbon spheres as efficient metal-free electrocatalysts for oxygen reduction reaction. Electrochim Acta 2015;178: 806–12.
[79] Mopoung S, Dejang N. Activated carbon preparation from Eucalyptus wood chips using continuous carbonization–steam activation process in a batch intermittent rotary kiln. Sci Rep 2021;11(1):1–9.
[80] Lozano K, Yang S, Jones RE. Nanofiber toughened polyethylene composites. Carbon 2004;42(11):2329–31.
[81] Horikawa T, Sakao N, Sekida T, Hayashi J, Do DD, Katoh M. Preparation of nitrogen-doped porous carbon by ammonia gas treatment and the effects of N-doping on water adsorption. Carbon 2012;50(5):1833–42.
[82] Liu L, Tan Shiliang J, Horikawa T, Do DD, Nicholson D, Liu J. Water adsorption on carbon - a review. Adv Colloid Interface Sci 2017;250:64–78.
[83] Villora-Picó JJ, Pastor-Blas MM, Sepúlveda-Escribano A. N-doped activated carbons from polypyrrole – effect of steam activation conditions. Chem Ing Tech 2022;94(1–2):94–100.
[84] Fletcher AJ, Uygur Y, Mark Thomas K. Role of surface functional groups in the adsorption kinetics of water vapor on microporous activated carbons. J Phys Chem C 2007;111(23):8349–59.
[85] Liu YC, Chen YW. Hydrogenation of P-chloronitrobenzene on lanthanum-promoted NiB nanometal catalysts. Ind Eng Chem Res 2006;45(9):2973–80.
[86] Wei P, Liang J, Liu Q, Xie L, Tong X, Ren Y, Li T, Luo Y, Li N, Tang B, Asiri AM, Hamdy MS, Kong Q, Wang Z, Sun X. Iron-doped cobalt oxide nanoarray for efficient electrocatalytic nitrate-to-ammonia conversion. J Colloid Interface Sci 2022;615:636–42.
[87] Hu X, Long Y, Fan M, Yuan M, Zhao H, Ma J, Dong Z. Two-dimensional covalent organic frameworks as self-template derived nitrogen-doped carbon nanosheets for eco-friendly metal-free catalysis. Appl Catal, B 2019;244:25–35.